Thermal Behavior and Phase Morphology of Miscible Hydrogen-Bonded Blends of Poly(ε-caprolactone) and Enzymatically Polymerized Polyphenol

Jianchun Li,[1] Tokuma Fukuoka,[2] Yong He,[1] Hiroshi Uyama,[3] Shiro Kobayashi,[2] Yoshio Inoue[1]

[1]*Department of Biomolecular Engineering, Tokyo Institute of Technology, Nagatsuta 4259-B-55, Midori-ku, Yokohama 226-8501, Japan*
[2]*Department of Materials Chemistry, Kyoto University, Nishikyo-ku, Kyoto 606-8510, Japan*
[3]*Department of Materials Chemistry, Osaka University, Yamadaoka 2–1, Suita, Osaka 565-0871, Japan*

Received 13 April 2005; accepted 1 September 2005
DOI 10.1002/app.23153
Published online in Wiley InterScience (www.interscience.wiley.com).

ABSTRACT: Enzymatically prepared novel polyphenol poly(4,4′-dihydroxydiphenyl ether) (PDHDPE) is blended to modify the properties of biodegradable polyester poly(ε-caprolactone) (PCL). Since the differential scanning calorimetry data show single composition-dependent glass transition for each blend, PCL and PDHDPE are found to be miscible in the amorphous phase. The crystallization of PCL is depressed by PDHDPE because PDHDPE reduces the molecular mobility and the flexibility of molecular chains of PCL. The Fourier transform infrared spectra clearly indicate that PCL and PDHDPE interact through strong intermolecular hydrogen bonds formed between the carbonyl groups of PCL and the hydroxyl groups of PDHDPE. The increase of the long period, calculated on the basis of Bragg's law with the measurement of small-angle X-ray scattering, is found because the peak position of the profiles of Lorentz-corrected intensity shifts to smaller angle. With the help of lamellar stack model and one-dimensional correlation function, the accurate lamellar parameters are calculated. The increase of long period is induced by the increase of crystal thickness. The thermal treatment can effectively modify the thermal stability of PCL/PDHDPE blends with the introduction of an intermolecular coupling of the polymer to give crosslinked and/or branched products. It is also found that the addition of PDHDPE to PCL would obviously increase the Young's modulus of PCL. © 2006 Wiley Periodicals, Inc. J Appl Polym Sci 101: 149–160, 2006

Key words: biodegradable; blends; equilibrium melting temperature; hydrogen bond; miscibility

INTRODUCTION

Phenol–formaldehyde resins, such as novolaks and resols, are synthesized by the condensation of phenol and formaldehyde, and are widely used in industry because of their low manufacturing cost, dimension stability, high tensile strength, and flame retardance.[1] However, an alternative process without formaldehyde to prepare phenol polymers has been strongly desired due to the toxic nature of formaldehyde.

Recently, the area of in vitro enzyme-catalyzed organic reactions has received great attention, since many families of enzymes can be utilized for transformation of not only their natural substrates but also a wide range of unnatural compounds, yielding a variety of useful materials. Enzymatic polymerization is defined as chemical polymer synthesis in vitro (in test tubes) via nonbiosynthetic (nonmetabolic) pathways catalyzed by an isolated enzyme.[2] The main target macromolecules of the enzymatic polymerization are polysaccharides, polyesters, poly(amino acid)s and polyaromatics.[3]

Enzymatic polymerization of phenols has been extensively investigated and this method is thought of as an environmentally benign production process. First, the polymerization of the phenols are catalyzed by enzymes usually under mild reaction conditions; in most cases, in water at neutral pH at a low temperature with a high quantitative conversion, high catalytic activity, high selectivity (substrate-, stereo-, regio-, chemo-, etc.), and no undesirable side products.[4] Second, because the polyphenols are generated by an enzymatic process and based on analogies with the biological heteropolymers like lignin and humic acid, it is reasonable to assume the biodegradability of polyphenols. Actually, the assumption has been confirmed by the soil-system biodegradation of poly(*p*-ethyl phenol), poly(*m*-cresol), and poly(*p*-phenylphenol), which are synthesized by peroxidase-catalyzed free-radical polymerization.[5] The enzymatically synthesized polyphenols have structures normally of a mixture of phenylene and oxyphenylene units.[6–9]

Recently, enzyme horseradish peroxidase (HRP), a single-chain β-type hemoprotein, has received a lot of

Correspondence to: Y. Inoue (yinoue@bio.titech.ac.jp).

attention because of its availability, stability, and wide substrate range.[10] HRP is commercially important and used as an effective catalyst for oxidative polymerization of 4,4′-dihydroxydiphenyl ether (DHDPE).[6,11] The reaction yield is as high as 83% and the synthesized polymer, poly(4,4′-dihydroxydiphenyl ether) (PDHDPE), shows high thermal stability with a decomposition temperature above 250°C.

On the other hand, it has been well realized that using biodegradable plastics like poly(ε-caprolactone) (PCL) is one of the ultimate available solutions to the environmental problems caused by the disposal of traditional nonbiodegradable plastic wastes. Blending is one of the important means to modify the properties of polyesters. The introduction of intermolecular hydrogen-bonding interaction has been a well-known strategy to enhance the compatibility of the polymer blends. The formation of intermolecular hydrogen bonds not only promises the miscibility of the polyester blends but also effectively modifies the properties of the polyesters. It has been reported that DHDPE with two phenolic hydroxyl groups has the ability to form the intermolecular hydrogen bonds with PCL and to modify PCL properties greatly.[12]

In the present article, the enzymatically polymerized polyphenol PDHDPE is used to modify the properties of biodegradable polyester PCL with the introduction of intermolecular hydrogen-bonding interaction. Here, polymer PDHDPE rather than the monomer DHDPE is expected to more effectively modify the thermal and mechanical properties of PCL. PDHDPE has the same characteristic hydroxyl groups as its monomer DHDPE, which has the ability to form intermolecular hydrogen bonds with PCL. The polymer has better thermostability than the monomer in the process, since enzymatically polymerized polyphenol can be thermally cured at appropriate temperature under vacuum.[13] It is reasonable to expect that the addition of PDHDPE would greatly improve the Young's modulus of PCL, if a miscible blend system was achieved. The miscibility and isothermal crystallization kinetics are investigated for PCL/PDHDPE blends by differential scanning calorimetry (DSC). The specific interaction between PCL and PDHDPE is affirmed by Fourier transform infrared (FTIR) spectroscopy. The crystal structure and phase morphology of PCL in the blends are analyzed by wide-angle X-ray diffraction (WAXD) and small-angle X-ray scattering (SAXS), respectively. The thermal stability of PCL/PDHDPE blends is measured by thermogravimetry (TG). Finally, the mechanical properties of the blends are evaluated.

EXPERIMENTAL

Materials

The PCL powder sample (Celgreen® PH4, M_n = 1.37 × 10^5; M_w/M_n = 1.49) was supplied by the courtesy of Daicel Chemical Industries, Ltd. (Osaka, Japan). PDHDPE (M_n = 1100; M_w/M_n = 1.1) was prepared by peroxidase-catalyzed oxidative polymerization of DHDPE with HRP as catalyst in aqueous methanol.[6] The polymer precipitate has been purified with an aqueous methanol (50:50 vol%) to eliminate the low-molecular-weight monomer. PDHDPE consists of phenylene and oxyphenylene units (Scheme 1) with a low content of α,ω-hydroxyoligo(1,4-phenylene oxide)s.[11]

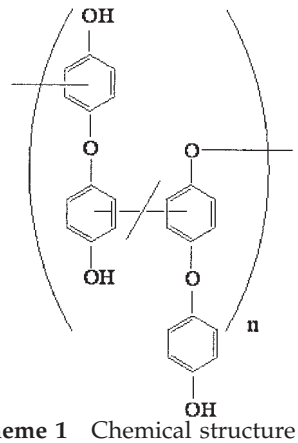

Scheme 1 Chemical structure of PDHDPE.

Preparation of blend samples

PCL/PDHDPE blend samples containing up to 40 wt% of PDHDPE were prepared by casting the 1,4-dioxane solution with concentration about 2 wt% on Teflon Petri dishes. The films were placed for 1 week under vacuum at room temperature to eliminate the solvent completely, and kept in an oven at 25°C for more than 2 weeks, which is long enough for the samples to reach thermodynamic equilibrium before characterization.

The thin layers of the PCL/PDHDPE blends with a thickness suitable for FTIR measurements were prepared by casting the 1,4-dioxane solutions on silicon wafers (Mitsubishi Materials Corp., Tokyo, Japan). The concentration of PCL in the solution was about 20 mg mL^{-1}. The silicon wafer used as a substrate was transparent for an IR incident beam. The maximum absorption of the resulting thin layer was within 1 absorbance unit, which ensured that all absorptions were within the linearity range of the detector. The FT-IR samples were placed one additional week under vacuum to eliminate the solvent completely and then kept in an oven for 2 weeks at 25°C.

Analytical procedures

Differential scanning calorimetry

DSC thermograms were recorded on a SEIKO DSC 220U instrument with the EXSTAR 6000 Station (Seiko

Instrument, Co., Tokyo, Japan) as follows: about 5 mg of a sample (PCL/PDHDPE blends) was encapsulated into an aluminum pan, and then heated from −90 to 180°C at a scanning rate of 20°C min^{-1} (the first heating scan). The sample was rapidly quenched to −100°C by liquid nitrogen, and reheated from −90 to 180°C also at a scanning rate of 20°C min^{-1} (the second heating scan).

The melting point T_m (first) was taken as the endothermic peak top in the thermal diagram recorded by the first heating scan, and the melting enthalpy (ΔH) (first) was calculated from the integral of the endothermic melting peak in DSC curve. The glass-transition temperature T_g (second) was taken as indicated by differentiation of DSC (DDSC) peak recorded by the second heating scan.

Isothermal crystallization and measurement of equilibrium melting temperature were carried out with PYRIS Diamond DSC (PerkinElmer Japan Co., Ltd., Yokohama, Japan). The instrument was routinely calibrated with high-purity indium and N_2 was used as purge gas. All data acquisitions and analyses were performed using the PYRIS software package. The crystallization and subsequent melting behavior of samples (about 7 mg in mass) of PCL and PCL/PDHDPE blends were investigated from 25 to 41°C. Each sample was first melted at 180°C and held at this temperature for 2 min to erase any prior thermal history. Then, the sample was quenched (about 80°C min^{-1}) to the desired temperature (T_c) and held at this temperature to crystallize. After isothermal crystallization was completed, the sample was heated to 180°C at a rate of 10°C min^{-1} to measure the T_m of the isothermally crystallized sample.

FTIR measurements

FTIR measurements were carried out on a single-beam PerkinElmer Spectra 2000 FTIR spectrometer (PerkinElmer) at room temperature under N_2 purging. All spectra were recorded from 600 to 4000 cm^{-1} at a resolution of 4 cm^{-1} and with an accumulation of 64 scans.

Line-shape analysis of FTIR spectra

A curve-fitting program was applied to resolve the vibration bands of PCL carbonyl groups into three components: the amorphous, the crystalline, and the hydrogen-bonded components. This program is based on the least-squares parameter-adjustment criterion using the Gauss–Newton iteration procedure.[14] This fitting adjusts the peak position, the line shape, and peak width and height by a Gaussian–Lorentzian combined line shape function to obtain the best fit.

Wide-angle X-ray diffraction and small-angle X-ray scattering

WAXD patterns of the blend films were recorded by a RINT-2000 X-ray diffractometer (Rigaku Corp., Tokyo, Japan) using Nickel-filtered Cu-Kα radiation ($\lambda = 0.154$ nm; 40 kV; 200 mA) with the 2θ incident angle ranging from 5 to 50° at a scanning rate of 1° min^{-1}. SAXS measurements were carried out on the same instrument. Scans were made between Bragg angles of 0.1–2.5°. The intensity was recorded per 0.004°, and X-rays were controlled for 4 s at one step.

Thermogravimetry

TG thermograms were recorded on a SEIKO TG/DTA 220U instrument with the EXSTAR 6000 Station (Seiko Instrument, Co., Tokyo, Japan) as follows: about 5 mg of a sample (PCL/PDHDPE blends) was encapsulated into an aluminum pan, kept at 50°C, and heated from 50 to 500°C at a heating rate of 5°C min^{-1} with a nitrogen flow rate of 300 mL min^{-1}.

Tensile test

Measurements of the mechanical properties of specimens were carried out at room temperature with a Shimadzu EZ Test machine (Shimadzu, Corp., Kyoto, Japan) at a cross-head speed of 5 mm min^{-1}. All samples had a gauge length of 22.25 mm, and a gauge width of 4.76 mm with variable thickness in the range of 0.2–0.3 mm. Each value of the mechanical properties reported was an average of three specimens. The Young's modulus E was obtained from the tangent of the initial slope of force versus elongation curve.

RESULTS AND DISCUSSION

DSC analysis of PCL/PDHDPE blends

It is well recognized that the observation of a single composition-dependent T_g between those of the neat polymer components can be taken as the evidence of miscibility.[15] Since the glass transition of a polymer takes place in the amorphous phase, for a semicrystalline polymer like PCL, the accurate value of T_g can be obtained by the second heating scan of DSC measurement as described in the experimental part to eliminate or weaken the influence of the amorphous rigid interfacial region situated between the lamellar crystals and the amorphous phase.

Figure 1 shows the DSC traces of PCL/PDHDPE blends with various contents of PDHDPE recorded during (A) the first and (B) the second heating scans. In the first scan, the DSC trace of PCL shows an endothermic peak at 62°C, which is attributed to the melting of the crystalline domain. Since the glass tran-

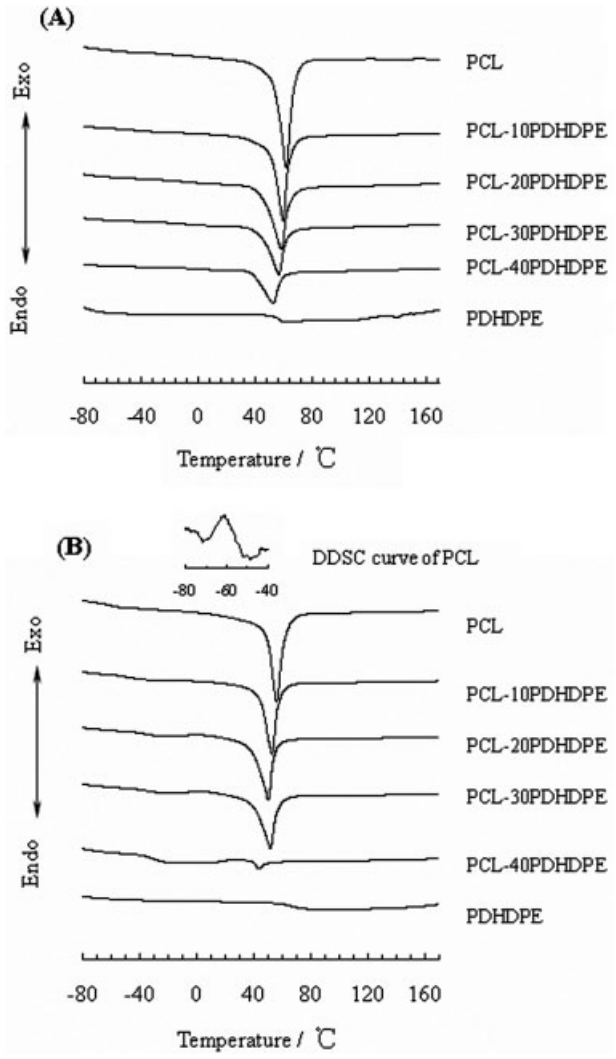

Figure 1 DSC curves of PCL, PDHDPE, and their blends recorded during the first (A) and the second (B) heating scans at a scanning rate of 20°C min^{-1}.

sition of the amorphous domain of PCL (an increase of heat capacity) is not obvious (because of the high crystallinity of PCL), the T_g at −61°C is taken as indicated by DDSC peak recorded by the second heating scan. The crystallinity of PCL in the blend, X^*, can be estimated from the melting enthalpy, ΔH, in the first scan and the reference melting enthalpy of PCL with 100% crystallinity, ΔH_{ref}, via eq. (1):

$$X^* = \Delta H/(W_{PCL}\Delta H_{ref}) \times 100\% \quad (1)$$

where W_{PCL} is the weight percentage of PCL in the blend and ΔH_{ref} = 166 J g^{-1}.[16]

PDHDPE is an amorphous polymer with one T_g at 60°C. As shown in Figure 1(A), only one melting peak corresponding to the PCL component is observed for all the blends. With the increase of the content of PDHDPE, the T_m value of PCL decreases gradually from 62°C for neat PCL to 52°C for that in the blend with 40% PDHDPE. The decrease of the crystallinity of PCL is also observed, that is, from 48% (neat PCL) to 37% (PCL-40PDHDPE). These phenomena suggest that the existence of PDHDPE influences the crystallization of PCL. The T_g value of PCL in the blends evidently shifts to higher temperature as shown in Figure 1(B). With increasing content of PDHDPE from 0 to 40% in the blends, the T_g of PCL/PDHDPE increased from −61 to −31°C.

The thermal properties of PCL and its blends with PDHDPE are summarized in Table I. These changes of the thermal properties should be attributable to the existence of the interaction between PCL and PDHDPE. A probable interaction is the formation of hydrogen-bonding interaction between the carbonyl groups of PCL and the hydroxyl groups of oxyphenylene units of PDHDPE. Because of the formation of the intermolecular hydrogen bonds, the PDHDPE molecules might act as the physically attached bulky side groups of PCL chain in the blends. Furthermore, through the formation of the hydrogen-bonded network, PDHDPE might also act as a physical crosslinking agent in the blend. Both the physical bulky side groups and the crosslinks would lower the mobility and the flexibility of PCL chains, resulting in the T_g increasing.

Crystallization kinetics of PCL/PDHDPE blends

The crystallization of polymers of sufficient structural regularity can occur over a range of temperatures limited by T_g and T_m. The characteristic shape of the temperature–crystallization-rate curves is a consequence of growth being slowed by increasing viscosity at a temperature close to the T_g, and by diminishing thermodynamic driving force at temperatures close to the T_m.[17] The crystallization of PCL in the blends would lead to various degrees of crystallinity with the variation of crystallization temperature, which might

TABLE I
The Thermal Properties and Crystallinity of PCL/PDHDPE Blends

Sample	T_m/°C[a]	ΔH/J · g^{-1}	X^*/%[b]	T_g/°C[c]
PCL	62	78 ± 7	48 ± 5	−61
PCL-10PDHDPE	59	64 ± 6	43 ± 5	−54
PCL-20PDHDPE	58	55 ± 6	41 ± 5	−41
PCL-30PDHDPE	57	46 ± 5	39 ± 5	−35
PCL-40PDHDPE	52	37 ± 4	37 ± 4	−31

[a]Obtained from the DSC first heating scan.
[b]Calculated from the ΔH of the PCL component (the area of the DSC melting peak in the first heating scan), with the ΔH of 100% crystalline PCL assumed to be 166J · g^{-1}.[16]
[c]Obtained from the second heating scan.

have profound effects on its thermal and mechanical properties.

The Avrami equation is generally used to analyze the overall crystallization rate under isothermal conditions.[18–20] The general form of Avrami equation is:

$$1 - X_c = \exp(-Kt_c^n) \tag{2}$$

where t_c is the time elapsed after the onset of crystallization; K is a temperature-dependent crystallization rate constant containing the nucleation and growth rates; n is the so-called Avrami exponent, which depends on both the mode of nucleation and the dimensionality of the subsequent crystal growth; and X_c is the relative crystallinity, which can be calculated according to eq. (3):

$$X_c = \frac{\Delta H_c}{\Delta H_{\inf}} = \frac{\int_{t_0}^{t} (dH/dt)dt}{\int_{t_0}^{\infty} (dH/dt)dt} \tag{3}$$

where ΔH_c is the melting enthalpy of the sample at t_c and $\Delta H_{\inf}$ is the maximum melting enthalpy attained for the sample. Taking logarithms of eq. (3), eq. (4) is obtained.

$$\ln[-\ln(1 - X_c)] = \ln K + n \ln t_c \tag{4}$$

Plotting the left-hand side of the preceding against $\ln t_c$ should give a straight line of slope n and intercept $\ln K$. Figure 2 describes typical linearized Avrami plots of isothermal crystallization data obtained at various temperatures for PCL in Figure 2(A) and PCL-10PDHDPE blend in Figure 2(B). A very good linear relationship can be observed. This fact makes the calculation of the n and K values possible during the crystallizing process. The results for all the PCL/PDHDPE blends studied here are listed in Table II. It shows that, at relatively high temperature above 39°C, the value of n is about 3. When the temperature decreases or PDHDPE is added to PCL, the value of n decreases. A lower dimensionality of the growth unit is thought as the reason for the drop in the Avrami exponent.

The crystallization half-time ($t_{1/2}$) is defined as the time required to reach $X_c = 0.5$. From n and K, it can be calculated according to eq. (5):

$$t_{1/2} = \left(\frac{\ln 2}{K}\right)^{1/n} \tag{5}$$

Figure 3 shows, as expected, that $t_{1/2}$ decreases as T_c decreases because a larger supercooling accelerates

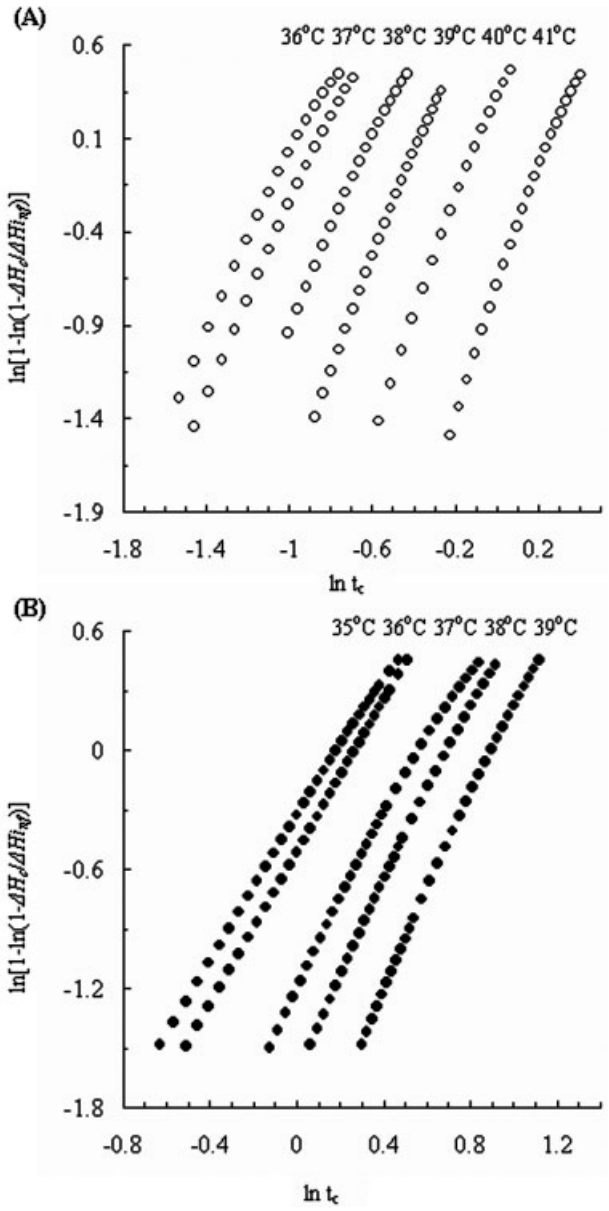

Figure 2 Typical linear Avrami plots showing the crystallization behavior of (A) PCL and (B) PCL-10PDHDPE blends.

the crystallization process for each composition. By examining the dependence of $t_{1/2}$ on the content of PDHDPE in the blends at the same temperature, the overall crystallization rate of PCL is depressed by the presence of PDHDPE because the mobility and the flexibility of PCL chains are reduced by PDHDPE, as suggested by the increase of T_g measured by DSC. However, some inconsistency is shown for PCL-10PDHDPE and PCL-15PDHDPE blends. It is thought that the effect of PDHDPE content on $t_{1/2}$ in the blends is less than that of crystallization temperature. Of course, the error, which is mainly produced in the calculation of n and K, cannot be neglected.

TABLE II
Avrami Parameters Obtained for PCL/PDHDPE Blends by Isothermal Crystallization

	PCL		PCL-10PDHDPE		PCL-15PDHDPE		PCL-20PDHDPE	
T_c/°C	n	K/min^{-n}	n	K/min^{-n}	n	K/min^{-n}	n	K/min^{-n}
25							1.7	1.2
27							1.9	8.6×10^{-1}
28							1.9	6.9×10^{-1}
29							1.9	5.4×10^{-1}
30					1.9	8.2	1.9	3.9×10^{-1}
31					2.0	7.9	1.9	2.9×10^{-1}
32					2.1	6.6		
33					2.1	4.5		
34					2.3	3.4		
35			1.8	7.1×10^{-1}				
36	2.3	9.8	1.9	6.0×10^{-1}				
37	2.5	9.0	2.0	3.1×10^{-1}				
38	2.5	5.0	2.2	2.1×10^{-1}				
39	2.9	3.3	2.4	1.2×10^{-1}				
40	3.0	1.4						
41	3.1	4.9×10^{-1}						

FTIR analysis of PCL/PDHDPE blends

FTIR spectroscopy is a quite suitable technique to investigate specific intermolecular interactions. The changes of the strength and wavenumber of IR absorption peaks resulting from some characteristic functional groups can be attributed to the existence of intermolecular interaction.

PDHDPE has an excellent potential as a proton donor for hydrogen-bonding interaction because of its phenolic hydroxyl groups. The monomeric repeating unit of PCL contains a carbonyl group, which yields a $\acute{\imath}_{C=O}$ stretching mode at 1728 cm^{-1} but PDHDPE has no group that produces absorption in the region from 1670 to 1770 cm^{-1}. Therefore, it is taken for granted that any changes in the FTIR spectra in this region

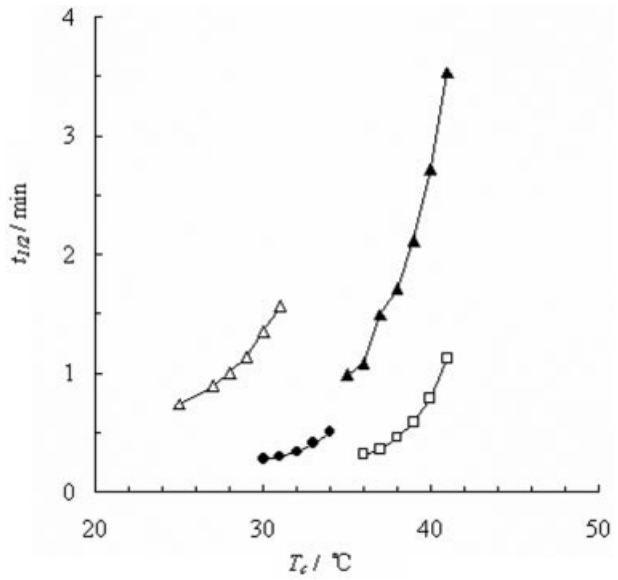

Figure 3 Crystallization half-time ($t_{1/2}$) as a function of T_c in different PCL/PDHDPE compositions: (△), PCL; (▲) PCL-10PDHDPE; (●) PCL-15PDHDPE; and (□) PCL-20PDHDPE.

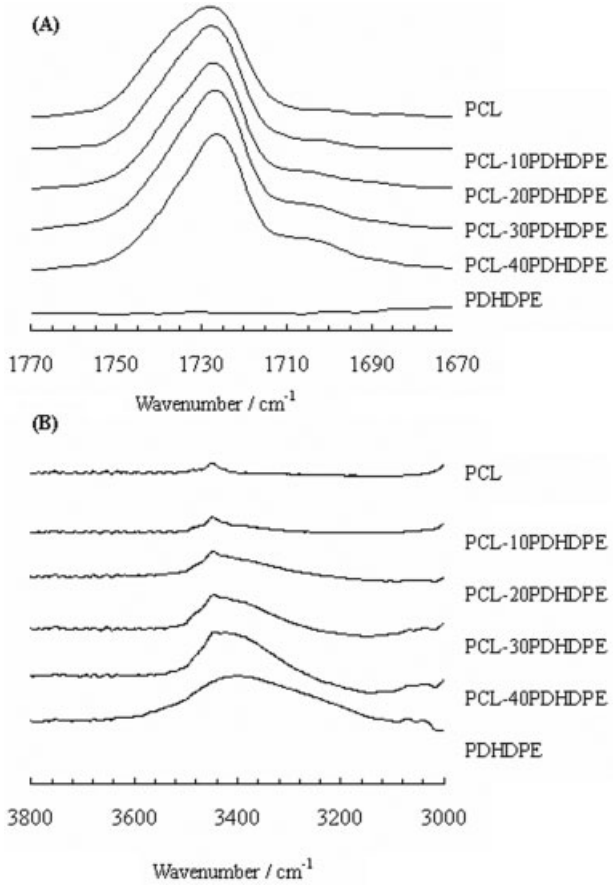

Figure 4 FTIR spectra of PCL, PDHDPE, and their blends with PDHDPE contents from 10% to 40%, in the vibration region of (A) carbonyl groups and (B) hydroxyl groups.

should be directly attributed to the change of the chemical environment of the carbonyl group, such as the formation of hydrogen bonds. As shown in Figure 4(A), when PCL is blended with PDHDPE, a new absorption band centered at ~1706 cm^{-1} appears, in addition to the band centered at 1728 cm^{-1}. The former band can be attributed to the vibration of the hydrogen-bonded ester carbonyl groups, indicating the formation of intermolecular hydrogen bonds between the carbonyl groups of PCL and the hydroxyl groups of PDHDPE. With increasing the content of PDHDPE, the relative absorbance of this hydrogen-bonded carbonyl group vibration increased and that of the free carbonyl group vibration is reduced, reflecting respectively the increase and the decrease of the percentage of the hydrogen-bonded and free carbonyl groups of PCL.

In Figure 4(B) are shown the FTIR spectral changes of PCL/PDHDPE blends in the vibration region of hydroxyl groups as the function of PDHDPE composition. In the spectrum for neat PDHDPE, a wide band centered at 3400 cm^{-1} appears, which should be mainly assigned to the free and the self-intermolecularly hydrogen-bonded hydroxyl groups in neat PDHDPE because of its low wavenumber. However, a very weak band centered at 3459 cm^{-1} is observed in this region and it should be attributed to the vibration of hydroxyl groups at the chain terminal of PCL. The contribution of this band to the whole spectra of blends studied here is negligible so long as the content of PDHDPE in the blends is not too low. When PCL is blended with PDHDPE, the vibration region of hydroxyl group is produced by three kinds of hydroxyl groups: the free, the self-intermolecularly hydrogen-bonded (PDHDPE—OH···OH—PDHDPE) and the intermolecularly hydrogen-bonded (PDHDPE—OH···O═PCL) hydroxyl groups. With increasing the content of PDHDPE in the blends, the peak of the band moves to lower wavenumber side and shows relatively higher absorbance, indicating the increase of the percentage of hydrogen-bonded hydroxyl groups with the PCL content decreasing.

In the PCL/DHDPE[12] and PCL/PDHDPE blend systems, there are four possible types of hydrogen-bonding interactions, i.e., the self-intermolecular one, DHDPE—OH···HO—DHDPE and PDHDPE—OH···HO—PDHDPE, and intermolecular one, DHDPE—OH···O═C—PCL and PDHDPE—OH···O═C—PCL. According to the observed wave number, the strength of these hydrogen-bonding interactions is in this order, i.e., DHDPE—OH···HO-DHDPE > PDHDPE-OH···HO-PDHDPE > DHDPE-OH···O═C—PCL ≈ PDHDPE—OH···O═C—PCL. Since the energy of hydrogen-bonding interaction of the DHDPE—OH···HO—DHDPE type is much higher than that of PDHDPE—OH···HO—PDHDPE type, it is easier for the PDHDPE—OH···HO—PDHDPE bond to break and form weaker hydrogen-bonding interaction with PCL.

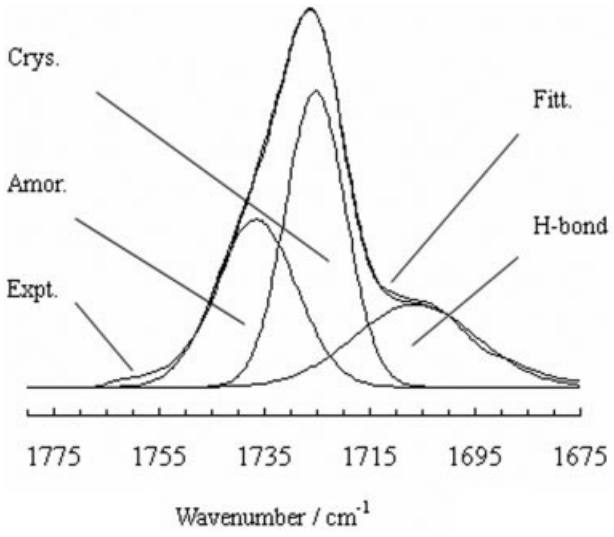

Figure 5 Experimental and fitted spectra for PCL-40PDHDPE blend in the carbonyl vibration region. Expt., experimental spectrum; Amor., amorphous component; Crys., crystalline component; H-bond, hydrogen-bonded component; Fitt., fitted spectrum; the sum of the amorphous, crystalline and hydrogen-bonded components.

Quantitative analysis of the fractions of hydrogen-bonded carbonyl groups

As discussed earlier, the formation of intermolecular hydrogen bonds between the carbonyl groups of PCL and the hydroxyl groups of PDHDPE has been confirmed qualitatively by FT-IR. Here, the Beer–Lambert law and a curve-fitting program are used to analyze quantitatively the formation of hydrogen bonds.[21]

As an example, Figure 5 illustrates the experimental and fitted spectra for the PCL-40PDHDPE blend in the vibration region of carbonyl group. The experimental spectrum can be divided into three peaks for the amorphous, the crystalline, and the hydrogen-bonded components at 1737, 1725, and 1706 cm^{-1}, respectively.[22] It is very easy to get the data of integrated intensity of them. The excellent agreement between the experimental and fitted spectra indicates the reliability of this fitting technique. The fraction of the carbonyl groups involved in the intermolecular hydrogen bonds ($F_{(B,CO)}$) could be calculated according to eq. (6):[23,24]

$$F_{(B,CO)} = A_{(B,CO)}/(A_{(B,CO)} + A_{(A,CO)}\gamma_{B/A} + A_{(C,CO)}\gamma_{B/C}) \quad (6)$$

where $A_{(B,CO)}$, $A_{(A,CO)}$, and $A_{(C,CO)}$ are the integrated intensities corresponding to the bands of the hydrogen-bonded, the amorphous, and the crystalline carbonyl group, respectively. $\gamma_{B/A}$ and $\gamma_{B/C}$ are the absorption ratios when the difference between the absorbances of the hydrogen-bonded and the amorphous carbonyl groups and that between those of the hydrogen-bonded and the crystalline carbonyl

TABLE III
The Relative Intensities and the Fractions of the Hydrogen-Bonded Carbonyl Groups in PCL/PDHDPE Blends

Sample	$A_{(A,\,CO)}/\Sigma A \times 100/\%$	$A_{(C,\,CO)}/\Sigma A \times 100/\%$	$A_{(B,\,CO)}/\Sigma A \times 100/\%$	$F_{(B,\,CO)}$
PCL	49 ± 2	51 ± 2	0	0
PCL-10PDHDPE	44 ± 1	50 ± 2	6 ± 1	0.04
PCL-20PDHDPE	40 ± 1	45 ± 1	15 ± 1	0.10
PCL-30PDHDPE	38 ± 1	43 ± 1	19 ± 1	0.13
PCL-40PDHDPE	33 ± 1	43 ± 1	24 ± 1	0.16

groups, respectively, are considered, since it has been shown that the absorption coefficient is a function of the frequency shift.[25] They are defined as:

$$\gamma_{i/j} = \int_0^{+\infty} \varepsilon_i(v)dv \Big/ \int_0^{+\infty} \varepsilon_j(v)dv \qquad (7)$$

where $\varepsilon_i(\nu)$ and $\varepsilon_j(\nu)$ are the absorbances of i and j components, ν is the wavenumber, and i and j are A, B, or C. On the assumption that neat PCL would not change its crystallinity in a narrow crystallization temperature range (45–50°C), $A_{(C,CO)}$ and $A_{(A,CO)}$ have a linear relationship with a slope $\gamma_{C/A}$, which can be accurately measured to be 1.46 through monitoring the changes of $A_{(C,CO)}$ and $A_{(A,CO)}$ during isothermal crystallization from the melt state with time-resolved FT-IR spectroscopy.[14] In the same way, in the amorphous PCL blend with hydrogen bonds ($A_{(C,CO)}$ is zero.), $A_{(B,CO)}$ and $A_{(A,CO)}$ have a linear relationship with a slope $\gamma_{B/A}$, which can be accurately measured to be 1.95. By dividing $\gamma_{B/A}$ by $\gamma_{C/A}$, $\gamma_{B/C}$ is calculated to be 1.34.[26]

Based on the theoretical analysis, in Table III are shown the data of the fractions of the hydrogen-bonded, the amorphous, and the crystalline carbonyl groups of the PCL/PDHDPE blends. It is found that the fraction of integrated intensity corresponding to the crystalline carbonyl group of neat PCL ($A_{(C,CO)}/\Sigma A \times 100\%$) is 51%. Compared to the crystallinity values by DSC, the slight difference is attributed to the fact that the IR crystallinity is based on preferred conformation. With increasing content of PDHDPE, the fraction of the hydrogen-bonded carbonyl groups ($A_{(B,CO)}/\Sigma A \times 100\%$) and $F_{(B,CO)}$ increase notably. When the percentage of PDHDPE arrives at 40%, $F_{(B,CO)}$ is 0.16, which is slightly higher than that in the PCL/DHDPE blend (0.13).[12] This result shows that PDHDPE has more ability than DHDPE to form intermolecular hydrogen bonds with PCL even though the content of hydroxyl group in the PCL-40PDHDPE blend is lower than that in the PCL-40DHDPE blend. This is explained by two reasons, i.e., the self-intermolecular hydrogen-bonding interaction among DHDPE molecules is too strong to break and to reform the intermolecular hydrogen bonds between DHDPE and PCL; furthermore, the much strong hydrogen-bonding interaction does not benefit the dispersion of DHDPE in PCL.

WAXD analysis of crystal structure

In Figure 6 are shown the typical WAXD patterns of solution-cast PCL and its blends with PDHDPE. It is clear that in the blends the crystalline structure of PCL is the same as that of neat PCL. Thus, it is thought that the addition of PDHDPE could not change the crystalline structure of PCL, although the formation of intermolecular hydrogen bonds between PCL and PDHDPE has been confirmed by DSC and FT-IR measurements. However, the WAXD patterns of the blends show that the content of amorphous component obviously increases with increasing the content of PDHDPE in the blends.

Lamellar morphology analyzed by SAXS

For a semicrystalline blend, the clarification of the location of amorphous component in the microphase is important, since it would affect distinctively the properties of the blend. In Figure 7 is shown the profiles of Lorentz-corrected intensity (Is^2) of semicrystalline PCL and PDHDPE blends crystallized at 25°C for 2 weeks. It is observed that with the content of PDHDPE increasing, the peak position (s_{max}) shifts towards smaller angle, which is explained by the increase of the long period (L) calculated on the basis of Bragg's law. It is well known that in the lamellar stack model with sharp phase boundary, the long period represents the sum of the crystal thickness (L_c) and the amorphous layer thickness (L_a). The increase of L can be induced by the thickening of PCL crystal or the

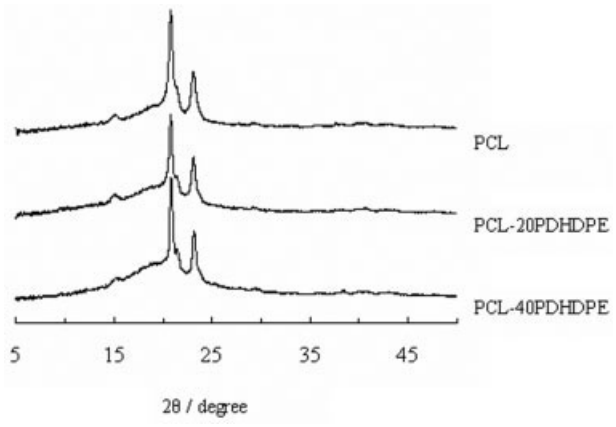

Figure 6 Wide-angle X-ray diffraction patterns for PCL and its blends with PDHDPE.

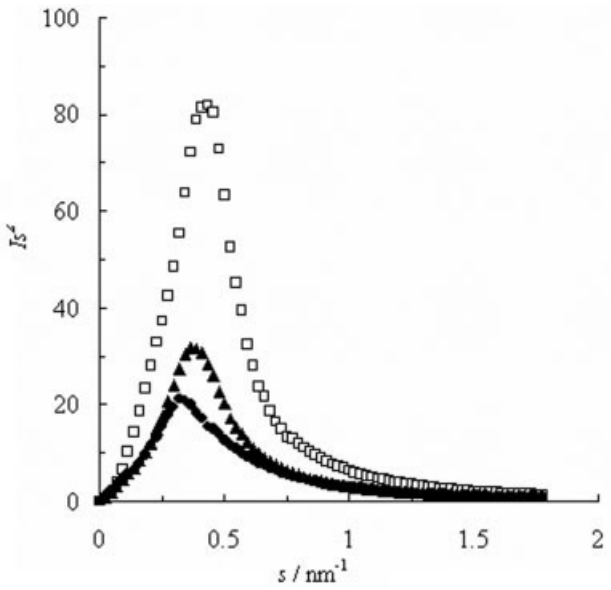

Figure 7 Lorentz-corrected SAXS intensities of PCL/PDHDPE blends isothermally crystallized at 25°C. (□) PCL, (▲) PCL-5PDHDPE and (●) PCL-10PDHDPE.

swelling of amorphous layers with the introduction of PDHDPE. One-dimensional correlation function $\gamma(r)$ defined as

$$\gamma(r) = \int_0^\infty sI(s)[J_0(2\pi rs) - 2\pi rsJ_1(2\pi rs)]ds \Big/ \int_0^\infty sI(s)ds \tag{8}$$

is used to calculate the average L, L_c, and L_a,[27] where r is the direction along the measured electron density, $s = 2\sin\theta/\lambda$, and J_n is a Bessel function of order n. When $\gamma(r)$ is related to the intensity function by Fourier transformation, the morphological parameters can be calculated from the direct graphical analysis of the correlation function. In Figure 8 is shown an inverse Fourier transform to the scattering relation for the experimental scattering profile for neat PCL as an example. A subtraction of thermal background, and an extrapolation to $s = 0$ by Guinier's law[28] and to ∞ by Porod's law[29–31] are carried out before the inverse Fourier transformation. The first maximum in $\gamma(r)$ is corresponding to L. Usually, the amorphous and crystalline layer thickness distribution do overlap, which would not bring a flat first minimum in the $\gamma(r)$ as shown in Figure 8. Here, a so-called quadratic expression as an alternative method is used to calculate the accurate values of L_a and L_c.[32] The intersection of the linear regression of self-correlation triangle with the abscissa always occurs at $r = \Phi(1 - \Phi)L$, where Φ and $1 - \Phi$ are the volume fractions of the crystalline and amorphous phases in the semicrystalline stacks. Since the expression is a quadratic, it yields two solutions for Φ, i.e., one solution Φ with a value below 0.5 and the other solution $1 - \Phi$ with a value above 0.5. The thickness of the thinner layer is $L_1 = L\Phi$ and that of the thicker one is $L_2 = L(1 - \Phi)$. Here, linear crystallinity Φ_c^{lin} is defined as:

$$\Phi_c^{lin} = L_c/L = L_c/(L_c + L_a) \tag{9}$$

when Φ_c^{lin} is less than 0.5, L_1 is L_c, and L_2 is L_a. The reverse is true when Φ_c^{lin} is more than 0.5. When the whole volume is homogeneously filled with lamellar stacks, Φ_c^{lin} equals to the bulk crystallinity, Φ_c, when the sample is not homogeneously filled, Φ_c^{lin} is larger than Φ_c. The value of Φ_c is assumed as the mass crystallinity and estimated from the melting enthalpy by the DSC measurement; however, this method is the unreliable for linear crystallinities in the range from roughly 0.3 to 0.7. For PCL blend systems, it is widely accepted that the crystal phase is assigned to the thicker length.[33–36] Furthermore, for a similar blend system (PCL/4,4′-thiodiphenol), it has been indicated that, if L_1 is assigned to L_c, the linear crystallinity is smaller than bulky crystallinity, which has no physical significance.[37] So, it is reasonable to assign L_1 to L_a and L_2 to L_c. In Table IV are listed the detailed lamellar parameters calculated with the one-dimensional correlation function for neat PCL and PCL/PDHDPE blends isothermally crystallized at 25°C. With increasing the content of PDHDPE, the values of L and L_c increase while that of L_a keeps almost constant. It suggests that the increase of L is induced by the increase of L_c, and the PCL/PDHDPE blends contain thicker lamellar than that of neat PCL.

Usually, the thicker crystal phase would induce the higher melting temperature of a polymer. Although the crystal phase becomes thicker with the addition of PDHDPE, the melting temperature shows contrary

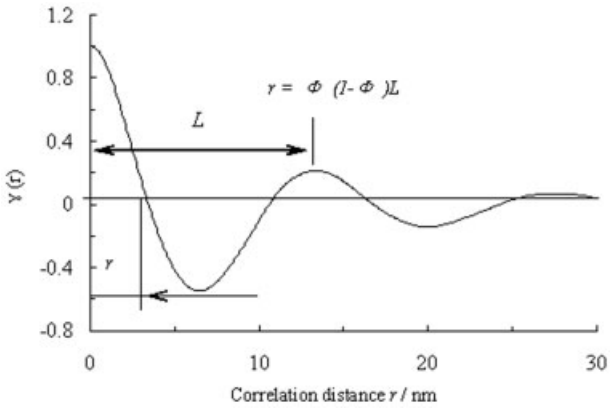

Figure 8 Graphical representation of one-dimensional correlation functions for neat PCL isothermally crystallized at 25°C.

TABLE IV
The Lamellar Parameters Calculated with the One-Dimensional Correlation Function PCL/PDHDPE Blends[a]

Sample	L/nm[b]	L_a/nm[c]	L_c/nm
PCL	14.0	6.1	7.9
PCL-5PDHDPE	14.1	6	8.1
PCL-10PDHDPE	14.7	6.1	8.6

[a]Isothermally crystallized at 25°C for two weeks.
[b]The first maximum in $\gamma(r)$ corresponding to the average long period L.
[c]Using the quadratic $r = \Phi(1 - \Phi)L$ to get two solutions, Φ and $1 - \Phi$ ($\Phi > 0.5$). $L\Phi$ equals to the average crystalline thickness L_c and $L(1 - \Phi)$ equals to the average amorphous thickness L_a.

tendency, that is, the melting temperature decreases. It is explained that the melting temperature of PCL in the blend depends not only on the crystal thickness but also on the perfection of crystal phase. With the addition of PDHDPE into PCL, the perfection of crystal phase is reduced, which would decrease the melting temperature of PCL. Therefore, the thicker crystal phase does not induce higher melting temperature consequentially.

Thermogravimetric analysis of PCL/PDHDPE blends

TG measurements are carried out under nitrogen for the normal samples (not thermally treated) and treated samples (thermally treated at 200°C for 5 h in a vacuum oven). Here, a temperature, at which the weight loss of sample is 5% measured by TG, is defined as thermal degradation temperature, T_d. In Figure 9 are shown the TG traces of (A) PCL, (B) PCL-40PDHDPE, and (C) PDHDPE samples, which are thermally treated or not treated. The two curves of neat PCL are almost overlapped, which suggest that thermal treatment would not produce obvious thermal degradation, since the T_d of neat PCL sample is above 350°C.[38] To neat PDHDPE, its T_d is found to be about 250°C, which may be due to the evaporation and/or evolution of low-molecular-weight compounds. When PCL/PDHDPE blends are thermally treated, the T_d increases from 250 to 310°C for neat PDHDPE, while the T_d increases from 323 to 344°C for PCL-40PDHDPE, the value of which is very close to that of neat PCL. It is concluded that the thermal treatment can effectively modify the thermal stability of PCL/PDHDPE blends.

It is known that conventional phenol resins (novolak and resol) have hydroxymethyl groups in the side chain, which involve the crosslinking reaction by a thermal treatment.[39] It is also reported that PVPh is subjected to thermal curing; however, the reaction mechanism is not clear yet. The crosslinking probably proceeds via the formation of phenoxy radicals, followed by an intermolecular radical coupling, or through the intermolecular dehydration of phenolic group.[40,41] It is thought that the thermal treatment make PDHDPE crosslinked, since the chemical structure of PDHDPE has some similar characteristics with those of novolak, resol, and PVPh. The measurement on the solubility of PDHDPE before and after thermal treatment confirms the assumption. PDHDPE is completely soluble in 1,4-dioxane, while the ratio of the dioxane-soluble part of the thermally treated PDHDPE is 22.4%. It is suggested that the thermal treatment induce an intermolecular coupling of the polymer to give crosslinked and/or branched products.

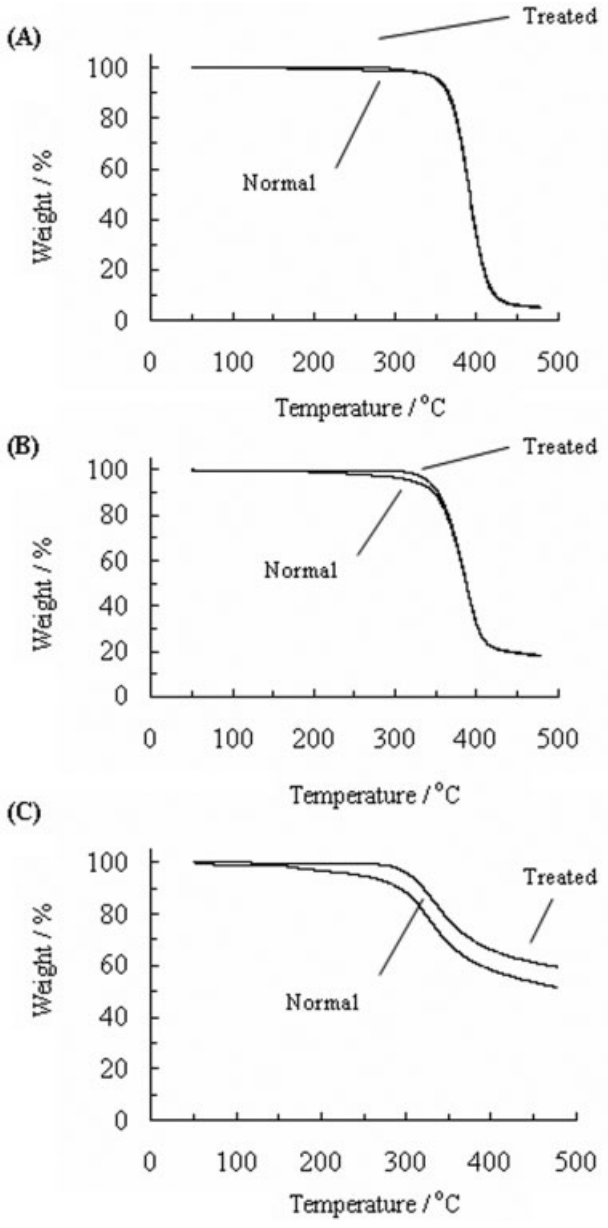

Figure 9 TG curves of PCL, PDHDPE, and their blends (A) PCL, (B) PCL-40PDHDPE, and (C) PDHDPE at a scanning rate of 5°C min^{-1}.

Mechanical properties of PCL/PDHDPE blends

The mechanical properties of PCL and its blends with PDHDPE are measured by tensile test and evaluated from the stress–strain curves. A stress–strain curve of PCL is shown as an example in Figure 10 to indicate the calculation of maximum strength (σ_{max}), elongation at break (ε_b), and Young's modulus (E). The results are presented in Table V.

It is obvious that the PCL, as well known, is a ductile polymer with significantly large ε_b and able to undergo large deformations. Unfortunately, it possesses a relatively low modulus, which renders its applications in wider fields where a high rigidity is required. As the DSC measurement indicates, the amorphous PDHDPE acts as a physical crosslinking agent in the PCL phase and the E of the blends can be improved significantly from 212 MPa (neat PCL) to 276 MPa (PCL-40PDHDPE) as shown in the Table V. Even though as a consequence other mechanical parameters like σ_{max} and ε_b are reduced, the blends have acceptable mechanical properties with respect to neat PCL.

TABLE V
The Mechanical Properties of PCL/PDHDPE Blends

Sample	Maximum Strength σ_{max}/MPa	Elongation at Break ε_b/%	Young's Modulus E/MPa
PCL	20 ± 2	681 ± 70	212 ± 21
PCL-10PDHDPE	17 ± 2	452 ± 45	221 ± 22
PCL-20PDHDPE	12 ± 2	378 ± 38	243 ± 34
PCL-30PDHDPE	11 ± 1	371 ± 37	268 ± 27
PCL-40PDHDPE	7 ± 1	336 ± 34	276 ± 28

CONCLUSIONS

A systematic study of the thermal behavior and phase morphology on the PCL/PDHDPE blends has been performed. It is found that the blends are miscible with the introduction of intermolecular hydrogen-bonding interaction, and the crystallization behavior of PCL in the blends is strongly influenced by the blend composition and the crystallization temperature. With the content of PDHDPE increasing, the long period of the blends increases due to the increase of crystal thickness. Thermal treatment can effectively improve the thermal stability of PDHDPE/PCL blends with the introduction of an intermolecular coupling of the polymer to give crosslinked and/or branched products. Furthermore, the addition of PDHDPE rather than its monomer DHDPE would not lose the good mechanical properties of PCL; on the contrary, the Young's modulus of PCL increases obviously. It is concluded that, with the introduction of hydrogen-bonding interaction, enzymatically polymerized polyphenol PDHDPE can effectively modify the properties of PCL.

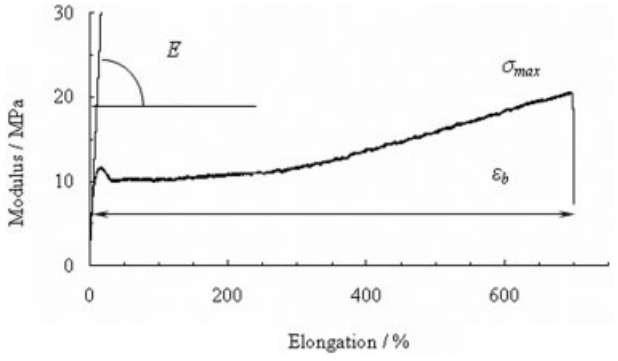

Figure 10 Stress–strain curve of PCL. ó$_{max}$, maximum strength, σ_b, elongation at break, and E, Young's modulus.

References

1. Ma, C.-C. M.; Wu, H. D.; Lee, C. T. J Polym Sci Part B: Polym Phys 1998, 36, 1721.
2. Kobayashi, S.; Uyama, H.; Kimura, S. Chem Rev 2001, 101, 3793.
3. Kobayashi, S.; Uyama, H.; Tonami, H.; Oguchi, T.; Higashimura, H.; Ikeda, R.; Kubota, M. Macromol Symp 2001, 175, 1.
4. Kobayashi, S. J Polym Sci Part A: Polym Chem 1999, 37, 3041.
5. Farrell, R.; Ayyagari, M.; Akkara, J.; Kaplan, D. J Environ Polym Degrad 1998, 6, 115.
6. Uyama, H.; Maruichi, N.; Tonami, H.; Kobayashi, S. Biomacromolecules 2002, 3, 187.
7. Fukuoka, T.; Tachibana, Y.; Yonami, H.; Uyama, H.; Kobayashi, S. Biomacromolecules 2002, 3, 768.
8. Ikeda, R.; Tanaka, H.; Uyama, H.; Kobayashi, S. Macromol Rapid Commun 2000, 21, 496.
9. Tonami, H.; Uyama, H.; Kobayashi, S. Biomacromolecules 2000, 1, 149.
10. Marx, K. A.; Zhou, T.; Sarma, R. Biotechnol Prog 1999, 15, 522.
11. Fukuoka, T.; Tonami, H.; Maruichi, N.; Uyama, H.; Kobayashi, S. Macromolecules 2000, 33, 9152.
12. Li, J.; He, Y.; Inoue, Y. J Polym Sci Part B: Polym Phys 2001, 39, 2108.
13. Kobayashi, S.; Uyama, H.; Ushiwata, T.; Uchiyama, T.; Sugihara, J.; Kurioka, H. Macromol Chem Phys 1998, 199, 777.
14. He, Y.; Inoue, Y. Polym Int 2000, 49, 623.
15. Bisso, G.; Casarino, P.; Pedemonte, E. Thermochim Acta 1998, 321, 81.
16. Chen, H. L.; Li, L. J.; Lin, T. L. Macromolecules 1998, 31, 2255.
17. Di Lorenzo, M. L.; Silvestre, C. Prog Polym Sci 1999, 24, 917.
18. Avrami, M. J Chem Phys 1939, 7, 1103.
19. Avrami, M. J Chem Phys 1940, 8, 212.
20. Avrami, M. J Chem Phys 1941, 9, 177.
21. Sanchis, A.; Prolongo, M. G.; Salom, C.; Masegossa, M. R. J Polym Sci Part B: Polym Phys 1998, 36, 95.
22. Li, J.; Zhu, B.; He, Y.; Inoue, Y. Polym J 2003, 35, 384.
23. Iriondo, P.; Iruin, J. J.; Fernandez-Berridi, M. J. Macromolecules 1996, 29, 5605.
24. Li, D.; Brisson, J. Polymer 1998, 39, 793.
25. Skrovanek, D. J.; Howe, S. E.; Painter, P. C.; Coleman, M. M. Macromolecules 1988, 21, 346.
26. He, Y.; Asakawa, N.; Inoue, Y. Macromol Chem Phys 2001, 202, 1035.

27. Balta-Calleja, F. J.; Vonk, C. G. In X-Ray Scattering of Synthetic Polymers; Elsevier: Amsterdam, 1989; p 175.
28. Guinier, A.; Fournet, G. Small-Angle Scattering of X-Rays; Wiley: New York, 1955.
29. Porod, G. Kolloid Z 1951, 124, 83.
30. Porod, G. Kolloid Z 1952, 125, 51.
31. Porod, G. Kolloid Z 1952, 125, 108.
32. Strobl, G. R.; Schneider, M. J. J Polym Sci Polym Phys Ed 1980, 18, 1343.
33. Russell, T. P.; Stein, R. S. J Polym Sci Polym Phys Ed 1983, 21, 999.
34. Vanneste, M.; Groeninckx, G.; Reynaers, H. Polymer 1997, 38, 4407.
35. Kuo, S.; Chan, S.; Chang, F. J Polym Sci Part B: Polym Phys 2004, 42, 117.
36. Chen, H.; Wang, S.; Lin, T. Macromolecules 1998, 31, 8924.
37. Zhu, B.; He, Y.; Yoshie, N.; Asakawa, N.; Inoue, Y. Macromolecules 2004, 37, 3257.
38. Pachence, J. M.; Kohn, J. In Principles of Tissue Engineering; Lanza, R. P., Langer, R., Chick, W. L., Eds.; Landes/Academic Press: Georgetown, TX, 1997; p 273.
39. Kopf, P. W. In Encyclopedia of Polymer Science and Engineering, 2nd ed.; Wiley: New York, 1986; Vol. 11, p 45.
40. Still, R. H.; Whitehead, A. J Appl Polym Sci 1977, 21, 1199.
41. Zhu, K. J.; Kwei, T. K.; Pearce, E. M. J Appl Polym Sci 1989, 37, 573.